Ocean Engineering 217 (2020) 107651

Contents lists available at ScienceDirect

Ocean Engineering

journal homepage: www.elsevier.com/locate/oceaneng

Systematic complexity reduction of wave-to-wire models for wave energy system design

Markel Penalba [b,a,*], John V. Ringwood [a]

[a] Centre for Ocean Energy Research, Maynooth University, Maynooth, Co., Kildare, Ireland
[b] Department of Mechanical and Manufacturing, Mondragon University, Loramendi 4 Apdo. 23, 20500, Arrasate, Spain

ARTICLE INFO

Keywords:
Wave energy
Wave-structure hydrodynamic interactions
Hydraulic power take-off
Wave-to-wire modelling
HiFiWEC
Systematic complexity reduction

ABSTRACT

Wave-to-wire models are valuable tools for a variety of applications in the development of successful wave energy converters. However, computational requirements of these wave-to-wire models are often prohibitive for certain applications that require fast mathematical models, such as power assessment or control design. The need for computationally fast models is traditionally achieved by assuming linear hydrodynamics and simplifying power take-off (PTO) dynamics with a linear damper in the mathematical model, though these assumptions can be relatively unjustified. However, these computationally appealing mathematical models can have a fidelity level which compromises their use in particular applications. Therefore, this paper suggests an application-sensitive *systematic* complexity reduction approach that reduces computational requirements of a high-fidelity simulation platform (*HiFiWEC*), *i.e.* a CFD-based numerical wave tank coupled to a high-fidelity PTO model, while retaining a level of fidelity in a sense specific to particular applications. The illustrative case study analysed here includes a point absorber with a hydraulic PTO system. Results show that reduced wave-to-wire models designed via the *systematic* complexity reduction approach retain the application-relevant fidelity (up to 95% fidelity compared to the *HiFiWEC*) for similar computational requirements shown by the traditionally used linear mathematical models.

1. Introduction

Ocean waves, with an untapped energy resource of about 32000 TWh worldwide (Mork et al., 2010), have the potential to become an alternative clean energy source contributing to the decarbonisation of the energy supply and the reduction of greenhouse emissions. However, the variability of the wave energy resource, along with the harsh environment in which wave energy converters (WECs) are deployed, poses an enormous challenge for WEC developers to design prototypes that can efficiently absorb the energy stored in ocean waves, while surviving such harsh conditions (Edenhofer et al., 2011).

Various different WECs based on diverse operating principles have been suggested to harvest wave energy, but none of the prototypes has shown economical viability yet. The different technologies can be classified based on the orientation and size of the WEC, the working principle (Falcão, 2010) or the location with respect to the shore (López et al., 2013). Fig. 1 illustrates different WECs, combining the three classifications.

To design successful devices, regardless of the type of WEC, an accurate understanding of the holistic performance of the WEC is vital. To that end, comprehensive mathematical models that include all the different stages of energy conversion from ocean waves to the electricity grid, are essential. These mathematical models are known in the literature as wave-to-wire (W2W) models. However, the computational complexity of comprehensive W2W models can be prohibitive for some wave energy applications where fast mathematical models are crucial. Computationally fast models traditionally employed in the literature assume linear hydrodynamics to represent wave-structure hydrodynamic interactions (WSHIs) and a linear damping model for the PTO system, regardless of the fidelity requirements of the application the W2W model is designed for. Indeed, such computationally appealing W2W models often produce poor results and, thus, are inadequate for certain applications. For example, the linear representation of WSHIs is demonstrated to be inaccurate for designing control strategies (Penalba et al., 2017a) and power production assessment (Mérigaud and Ringwood, 2018), and so is the linear damping representation of the PTO model for power assessment purposes (Penalba and Ringwood, 2018).

Therefore, this paper presents an alternative application-sensitive

* Corresponding author. Centre for Ocean Energy Research, Maynooth University, Maynooth, Co. Kildare, Ireland.
E-mail addresses: mpenalba@mondragon.edu (M. Penalba), john.ringwood@mu.ie (J.V. Ringwood).

https://doi.org/10.1016/j.oceaneng.2020.107651
Received 18 September 2018; Received in revised form 28 March 2020; Accepted 12 June 2020
Available online 18 September 2020
0029-8018/

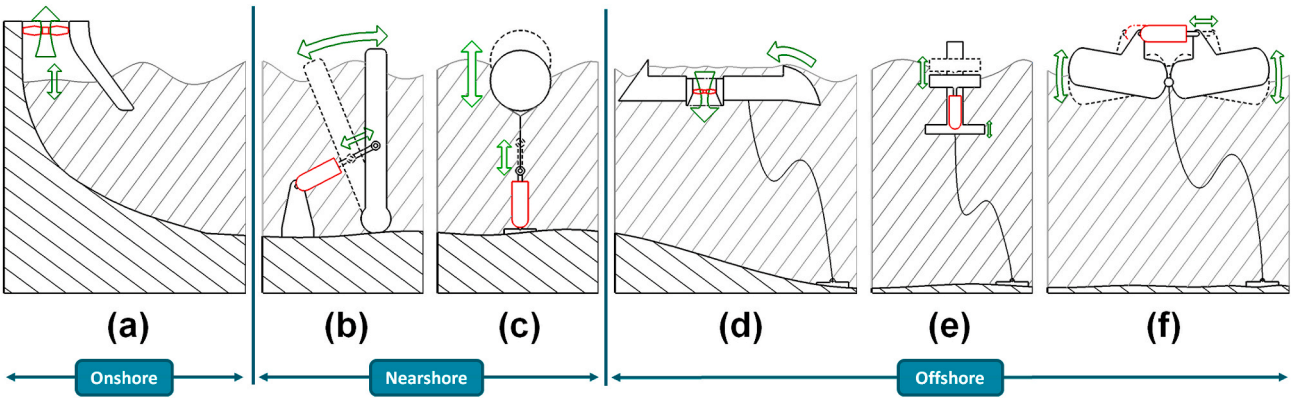

Fig. 1. The four different categories of WECs: (a) an onshore OWC, (b) a nearshore OWSC, (c) a nearshore point absorber, (d) an offshore overtopping device, (e) an offshore self-reacting point absorber and (f) an offshore attenuator.

Table 1
Specific requirements of the potential applications that demand W2W models.

Potential applications	Accuracy & Comp. cost		Specific dynamics & losses					Nonlinear effects
	Egen fidelity	Low comp. cost	WSHI	Transmission system dynamics	Transmission system losses	Electrical dynamics	Electric generator losses	
ValVer	+++	- - -	✓	✓	✓	✓	✓	
Ident	+++	- - -	✓	✓	✓	✓	✓	✓
SimWEC	++	-	✓	✓	✓	✓	✓	
PowSyst	++	-			✓	✓	✓	
MBC	++	+++			✓		✓	✓
PowAss	++	++			✓		✓	
PTOopt	++	++		✓	✓		✓	

systematic complexity reduction (CR) approach that starts with a reference high-fidelity, high-complexity W2W simulation platform, where a CFD-based numerical wave tank (CNWT) is coupled to a high-fidelity PTO model, such as the platform presented in (Penalba et al., 2018). Then, the complexity level is systematically reduced to an acceptable level, while attempting to maximally retain those fidelity aspects of the model crucial to the application. Hence, the W2W models designed via the *systematic* CR approach retain the maximum application-relevant fidelity, while moving into a computationally feasible range. This CR approach can be used for reducing the complexity level of any W2W model, regardless of the type of absorber and PTO system.

The remainder of the paper is organised as follows. Section 2 describes the different applications of W2W models and their specific requirements, Section 3 presents a critical literature review of existing W2W models, Section 4 describes the different CR techniques suggested in the literature, Section 5 presents the *HiFiWEC*, Section 6 describes the illustrative case study used in this paper, Section 6.1 introduces the *systematic* CR approach, including the set of balanced HyW2W models evaluated in this paper and the procedure to select the suitable HyW2W model for each application, Section 7 shows the results obtained for that set of balanced HyW2W models, and Section 8 draws a number of conclusions.

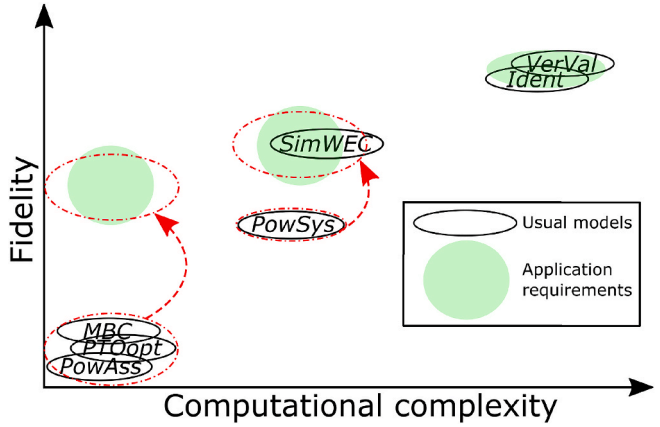

Fig. 2. Fidelity/complexity trade-off of application requirements and the modelling approaches commonly used for these applications.

2. Potential applications of wave-to-wire models

Specific applications of W2W models include validation of results obtained from simpler mathematical models or verification of the effectiveness of different control strategies (*ValVer*), identification of model parameters (*Ident*), simulation of WECs to evaluate their performance (*SimWEC*), modelling of electrical power systems and power quality analysis (*PowSyst*), design of upper-level model-based control strategies to maximise energy generation (*MBC*), assessment of WECs' power production capabilities (*PowAss*), and optimisation and sizing of PTO components (*PTOopt*).

All these specific applications have, in turn, specific requirements, as shown in Table 1, where *nonlinear effects* refers to the implications that nonlinear effects have in each application. For example, high-fidelity generated energy estimation (E_{gen}) is required for *ValVer* and *Ident*, including all the dynamics and losses from ocean waves to the electricity grid, and the computational cost (Comp. cost in Table 1) of the mathematical model is largely irrelevant, since only few simulations are normally computed in these applications. Requirements for *SimWEC* are similar to the requirements for *ValVer*, except for the computational cost, which cannot be prohibitively large for *SimWEC*. Similarly, modest computational cost is not the main requirement for *PowSyst*, but only losses in the transmission system and electric generator dynamics are necessary in the W2W model. In contrast, fast mathematical models are essential for *PowAss*, *PTOopt* and, particularly, *MBC*, while relatively high-fidelity E_{gen} is required in all three of these applications. In the case

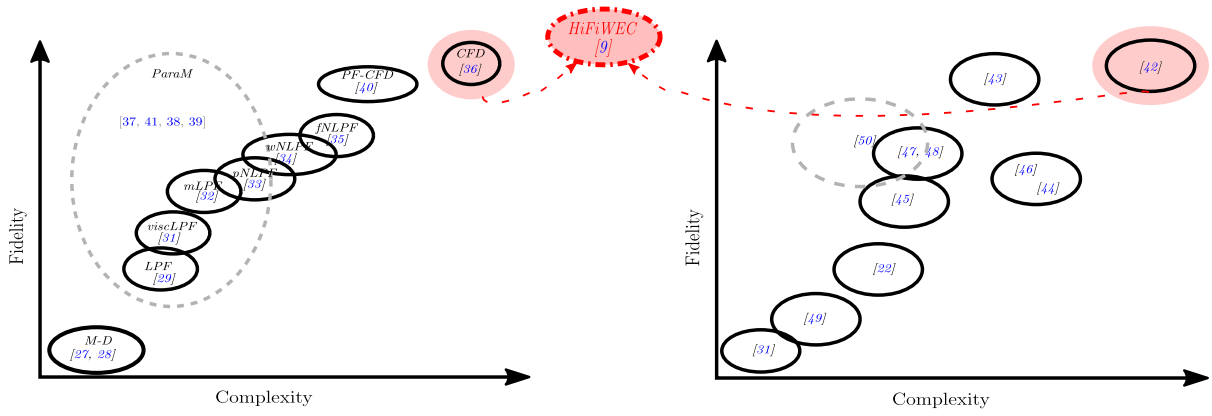

(a) WSHI modelling approaches, based on [30].

(b) HyPTO modelling approaches

Fig. 3. Fidelity/complexity trade-off of different modelling approaches for WSHIs (a) and the HyPTOs (b), where the grey colour refers to the lack of physical meaning of the modelling approach. The reader is referred to the electronic version for a correct interpretation of the color code. (For interpretation of the references to colour in this figure legend, the reader is referred to the Web version of this article.)

of *MBC* and *PowAss*, only the losses in the transmission system are necessary, while transmission system dynamics are also required for *PTOopt*. With respect to the impact of nonlinear effects, all the nonlinear effects must be covered by the W2W model used for *Ident*, while these nonlinear effects should be linearised whenever possible for *MBC*.

Table 1 shows that reasonably high-fidelity results are required in all the applications, while low computational cost requirements are quite restrictive for some applications. However, combining high-fidelity and low computational cost in a mathematical model is a challenging task. As a consequence, the fidelity of the numerical models used in certain applications is substantially lower than the fidelity required to obtain accurate results. This gap is particularly important for the applications where computationally fast models are required. Fig. 2 illustrates the fidelity/complexity compromise of the application requirements and the modelling approaches commonly used for these applications, illustrating the gap between the two in terms of fidelity.

3. Critical survey of existing wave-to-wire models

Accurate W2W models should include all the important dynamics, losses and constraints of the different conversion stages from waves to the electricity grid. However, the level of detail included in each subsystem varies significantly among the different W2W models in the literature.

Wave-to-wire models for different WECs and types of PTO system have been suggested in the literature. Oscillating water column devices with air-turbines coupled to electric generators are modelled in (Amundarain et al., 2011; Garrido et al., 2015; Henriques et al., 2016; Bailey et al., 2016; Kelly et al., 2016), while examples of wave-activated PAs coupled to PTO mechanism with mechanical transmission systems and linear generators are presented in (Tedeschi et al., 2011; Sjolte et al., 2013) and (Polinder et al., 2004; Wu et al., 2008; O'Sullivan and Lightbody, 2017), respectively. The details of the W2W models mentioned in this paragraph are critically analysed in (Penalba and Ringwood, 2016).

However, hydraulic PTO systems (HyPTO), composed of a hydraulic transmission system coupled to a rotary electric generator, appear to be the choice of the vast majority of WEC developers, including Pelamis (Henderson, 2006), Searev (Josset et al., 2007), Wavestar (Hansen et al., 2014), Oyster (Henry et al., 2010), CETO (Fiévez and Sawyer, 2015) and Waveroller (Lucas et al., 2012). Therefore, the illustrative case study analysed in the present paper, to demonstrate the capabilities of the *systematic* CR approach, is based on W2W models that incorporate a hydraulic transmission system (HyW2W), as shown in Fig. 6 (a), where the HyW2W model is divided into three main stages: waves, WSHI, and HyPTO.

The vast majority of the HyW2W models suggested in the literature often incorporate high-fidelity into a specific component or stage, but fail to design a balanced (fidelity) parsimonious model. The main weakness of the HyW2W models suggested in the literature is, in general, the WSHI model. In the simplest version, the WSHI is represented as a mass-damper (*M-D*) system (Li and Belmont, 2014; Brekken, 2011), but the most widely used approach is the linear potential flow (*LPF*) model based on the Cummins' equation (Yu and Falnes, 1995). However, the *LPF* model is demonstrated to overestimate the motion of WECs and, as a consequence, the absorbed energy (Penalba et al., 2017a; Mérigaud and Ringwood, 2018). A number of modelling approaches have been suggested to improve the *LPF* model (Penalba et al., 2017b), such as the *LPF* model with a quadratic viscous term (*viscLPF*) (Babarit et al., 2012), the multi-linear potential flow (*mLPF*) model (Crooks, 2016), the partially- (*pNLPF*) (Giorgi and Ringwood, 2017a), weakly- (*wNLPF*) (Letournel, 2015) and fully-nonlinear potential flow (*fNLPF*) models (Grilli et al., 2001), or the well-known computational fluid dynamics (*CFD*) approach (Windt et al., 2018a). An alternative is presented in Babarit et al. (2009), where a panel-based potential flow model is combined with a *CFD* model. Parametric models (*ParaMs*) determined from experimental data or produced by a higher-fidelity numerical model have also been suggested to model WSHIs, including grey- (Davidson et al., 2015) and black-box approaches (Giorgi et al., 2016; Anderlini et al., 2017). Fig. 3 (a) illustrates the fidelity/complexity compromise of each modelling approach, where the darker grey suggests less physical interpretability. The space corresponding to *ParaMs* in Fig. 3 (a) is defined by a dashed oval and covers a much wider space than other approaches, which represents the uncertainty and the potential of *ParaMs*, respectively.

Hydraulic PTO models have also been represented in many different ways in the literature, from an ideal HyPTO that completely neglects all the dynamics and losses (Babarit et al., 2012), to a complete HyPTO model (*cHyPTO*) including all the important dynamics, losses and constraints (Penalba and Ringwood, 2019). In order to critically evaluate the suitability of HyW2W models, it is essential to consider the application for which the HyW2W models in the literature were originally designed.

For instance (Ricci et al., 2011), suggests a HyW2W model for *MBC* and *PowAss*, where the compressibility of the hydraulic fluid and losses in hydraulic components are excessively simplified or neglected, and the electric generator is represented by an ideal constant load torque. Similar models for *PowAss* are also presented in (Josset et al., 2007) and (Bailey et al., 2014), where the former also includes compressibility effects of the hydraulic system and the latter includes losses for the

hydraulic motor. In conclusion (Ricci et al., 2011; Josset et al., 2007; Bailey et al., 2014), miss or excessively simplify important losses and constraints in the HyPTO model, resulting in significant overestimation of E_{gen} (Penalba and Ringwood, 2018).

A HyW2W model is employed in (Cargo et al., 2014, 2016) for *PTOopt* and *MBC*. This HyW2W model includes losses in the hydraulic cylinder and motor, but neglects the electrical dynamics and losses. Therefore, the PTO system and the active HyPTO tuning strategy suggested in (Cargo et al., 2016) may not be adequate, since *PTOopt* and *MBC* require the losses of the electric generator to be articulated. The HyW2W model suggested in (Hansen et al., 2011) is also used for *PTOopt* and *MBC*, but includes losses in the electric generator and the power converters, providing more reliable results. The only missing aspect in (Hansen et al., 2011) are electrical dynamics, which are neglected via a steady-state representation of the electric generator.

Due to the computationally fast models required for *MBC* (Gaspar et al., 2016), suggests an adaptive neuro fuzzy inference system (ANFIS) to represent the losses in the hydraulic cylinder and motor. The HyW2W model suggested in (Gaspar et al., 2016) also neglects electrical dynamics in the electric generator and the efficiency is calculated with a polynomial approximation, using efficiency constants that represent part- (25% and 50% of the full load) and full-load operations of the electric generator. The HyPTO model presented in (Gaspar et al., 2016) for *MBC* seems to be appropriate from a complexity perspective, but the suitability of the HyPTO model strongly depends on the fidelity of the (black-box) ANFIS model, which is not clear from (Gaspar et al., 2016).

HyW2W models for *PowSyst* are suggested in (Garcia-Rosa et al., 2014) and (Forehand et al., 2015), where electrical dynamics and losses are included in both models. However, losses in the hydraulic system are either excessively simplified, represented with a constant power loss value (Garcia-Rosa et al., 2014), or neglected (Forehand et al., 2015), which results in overestimation of E_{gen}.

The *cHyPTO* model for *SimWEC* is presented in previous work (Penalba and Ringwood, 2019) by the same authors of the present paper, which is then coupled to a CFD-based numerical wave tank (CNWT) in (Penalba et al., 2018), creating the *HiFiWEC* for *ValVer*, *Ident* and *SimWEC*, as illustrated in Fig. 3. This *HiFiWEC* is used as the starting basis for the *systematic* CR approach presented in this paper.

4. Model complexity reduction

The complexity of a mathematical model ($\mathscr{C}$) depends on a number of aspects, such as the order of the dynamic system or the number of equations included in the model ($\mathscr{N}$), the nonlinearity degree of the system (χ), and the computational cost given by the time required to run the simulation ($\mathscr{T}$).

$$\mathscr{C} = f(\mathscr{N}, \chi, \mathscr{T}) \tag{1}$$

The determination of $\mathscr{N}$ and $\mathscr{T}$ is straightforward and χ can be calculated via the nonlinearity measures suggested in (Penalba and Ringwood, 2019). However, the weight of each component in $\mathscr{C}$ is very application-specific, meaning that a generic complexity measure is unattainable.

Complexity reduction techniques in the literature include model order reduction (MOR) approaches, linearisation techniques and identification of compact parametric models from experimental data or produced by a higher-fidelity numerical model. Different MOR techniques can be classified into two main groups (Antoulas et al., 2001). On the one hand, there exist singular-value-decomposition-based methods, such as the balanced truncation (Moore, 1981), the Hankel-norm approximation (Glover, 1984), or the proper orthogonal decomposition (POD) (Willcox and Peraire, 2002). An extension of the balanced truncation approach, the balanced POD, has also been recently suggested to deal with cases where a balanced truncation becomes complicated (Singler and Batten, 2009). On the other hand, MOR techniques based on approximation by moment matching have been

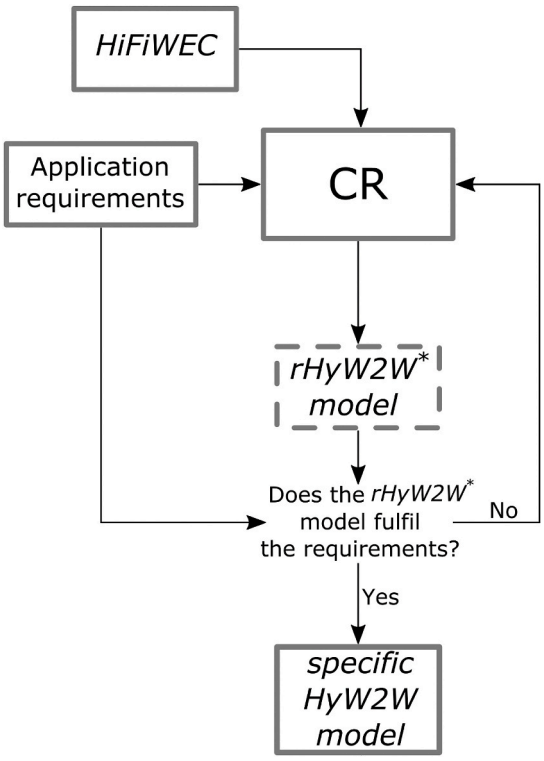

Fig. 4. The representation of an ideal but intractable *algorithmic* CR approach.

suggested (Astolfi, 2010), which are claimed to be numerically more efficient and reliable (Antoulas, 2005).

Specific to the wave energy field, research studies that apply these MOR techniques are scarce, to the best of authors' knowledge. For example (Hesam, 2014), applies the balanced POD technique to reduce a nonlinear WEC model implemented using a finite element method. The reduced-order model is then used to design an optimal controller for a WEC. Also with the aim of designing an optimal controller for a WEC, a model matching approach is applied to a linear WEC model in Faedo et al. (2018).

Linearisation techniques are used in several different fields (Cheng et al., 2010), providing a linear approximation of a nonlinear dynamical system around an operational point. However, due to the extreme variability of the wave resource, WECs do not have specific piecewise constant operating points, meaning that linearisation techniques are not as useful as in other fields. An extension to linearisation techniques in wave energy is the use of multi-linear or linear parameter-varying models, defining multiple linear models for different operational points and switching between these linear models, depending on the operational space. In this context, a pioneering approach is suggested in (Crooks, 2016), where the excitation force (F_{ex}) of a flap-device is calculated for several pitch angles, using the F_{ex} which depends on the position of the device at each time-step of the simulation.

Finally, parametric models can be identified from input/output data generated from real processes or high-fidelity numerical platforms (Ljung, 1999). The first issue with such parametric models is extracting or generating representative data from the process or numerical platforms, since this data must cover the whole range of frequencies and amplitudes the system will deal with. The second step, after the data is generated, is the selection of the model structure. Several model structures, from a linear autoregressive with exogenous input (ARX) models to nonlinear artificial neural networks (ANNs) can be selected. For example, linear parametric models, *e.g.* the ARX or the feedback block-oriented models, have been tested in (Davidson et al., 2015), where the incapacity to capture the nonlinear behaviour of WECs is reported. More complex model structures, which, in theory, are able to

represent nonlinear systems, *e.g.* Kolmogorov-Gabon polynomial (KGP) models, Hammerstein models, and ANNs, are also tested in (Giorgi et al., 2016), (Giorgi et al., 2015) and (Anderlini et al., 2017), respectively. However, these more complex model structures can result in overfitted parametric models (Giorgi et al., 2016).

Different reduced HyW2W (*rHyW2W*) models need to be designed for each application shown in Table 1, due to the specific requirements of each application. The ideal *rHyW2W* model for each application, referred to as the *specific HyW2W*model, would be generated by means of an *algorithmic* CR approach that considers the requirements of each application, as illustrated in Fig. 4. However, this *algorithmic* CR approach is intractable, due to the complexity of the *HiFiWEC*, the difficulty in quantifying and, as a consequence, reducing the application-specific complexity, and the difficulty in articulating application requirements. Therefore, a *systematic* CR approach is suggested in Section 6.1, progressively reducing the *HiFiWEC* model complexity.

5. The *HiFiWEC*

The *HiFiWEC* consists of a CNWT model that solves the fully nonlinear hydrodynamic WSHI coupled to the *cHyPTO* model (Penalba et al., 2018), as illustrated in Fig. 6 (a). Both the CNWT and the *cHyPTO* model have been validated against results obtained from wave tank experiments (Windt et al., 2018b) and test rigs (Penalba et al., 2017c, 2017d), respectively. The coupling between the CNWT and the HyPTO is also verified in (Penalba et al., 2018).

5.1. Wave model

Realistic ocean waves are polychromatic waves. The most established method to generate free-surface elevation time-series (η_w) for these polychromatic waves is by adding a finite number of sinusoidal Fourier components as follows,

$$\eta_w(t_i) = \sum_{k=1}^{N} A_k \cos(2\pi f_k t(t_i) + \varphi_k) \tag{2}$$

where t is the time vector, N the number of frequency components, f_k the frequency in Hz, $\varphi_k \in [0, 2\pi]$ the randomly chosen phase, $A_k = \sqrt{2S(f_k)\Delta f}$ the wave amplitude function, $S(f_k)$ the spectral density function that represents wave characteristics of a given location, and Δf the frequency step.

5.2. Wave-structure hydrodynamic interactions

In the *HiFiWEC*, η_w is the input for the CNWT, which is based on OpenFOAM (Weller et al., 1998), an open-source CFD software. Hence, the CNWT solves the fully-nonlinear behaviour of WECs by numerically solving the incompressible Reynolds Averaged Navier-Stokes (RANS) equations via a cell-centred finite volume method. The RANS equations describe the conservation of mass and momentum, respectively given as:

$$\nabla \cdot u = 0 \tag{3a}$$

$$\frac{\partial(\rho u)}{\partial t} + \nabla \cdot (\rho u u) = -\nabla p_f + \nabla \cdot T + \rho\, F_b \tag{3b}$$

where u is the fluid velocity vector, p_f the fluid pressure applied on the WEC, ρ the water density, T the stress tensor vector and F_b the external force vectors acting on the WEC, such as the gravity force (F_g) or mooring forces (F_{moo}). Further details about the CNWT implemented in the *HiFiWEC* are given in (Penalba et al., 2018). Hence, the output of the CNWT is the WEC motion, *i.e.* displacement (z_d), velocity ($\dot{z}_d$) and acceleration ($\ddot{z}_d$).

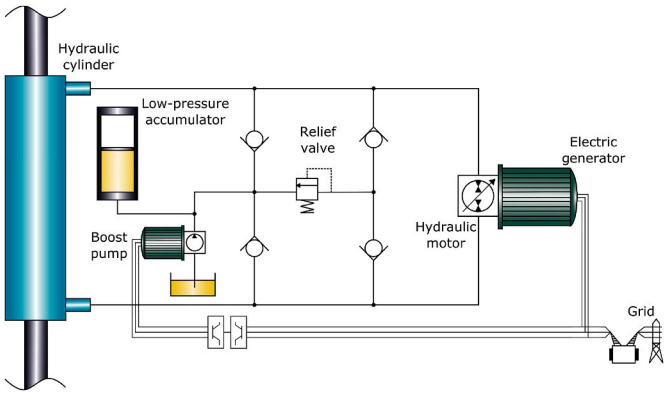

Fig. 5. Diagram of the PTO system implemented in the platform, including all the required components.

5.3. Power take-off system

Two different HyPTO configurations are commonly used in WECs, *i.e.* the constant- and variable-pressure configurations. However, for the sake of brevity, only the variable-pressure configuration is considered in this paper, which consists of a hydraulic cylinder, a low-pressure accumulator, relief valves and a variable-displacement hydraulic motor, coupled to a squirrel cage induction generator (SCIG) (Hansen et al., 2011), as illustrated in Fig. 5.

The mathematical model for the cylinder includes end-stop constraints, friction losses (F_{fric}), and fluid compressibility and inertia effects related to piston and fluid mass (F_I), providing the total piston force as follows,

$$F_{pis} = A_p \Delta p + F_{fric} + F_I \tag{4a}$$

where A_p is the piston area, Δp the pressure difference between the two chambers of the hydraulic cylinder, and

$$\dot{p} = \frac{\beta_{eff}}{V + A_p x_p}\left(Q - \dot{x}_p A_p\right), \tag{4b}$$

$$F_{fric} = \sigma_v \dot{x}_p + \text{sign}(\dot{x}_p)\left[F_c + F_{st}\exp\left(-\frac{|\dot{x}_p|}{c_{st}}\right)\right], \tag{4c}$$

$$F_I = \ddot{x}_p\left(M_p + M_r + M_{oil}\right). \tag{4d}$$

β_{eff} is the effective bulk modulus, V the minimum volume in the cylinder chamber, x_p, $\dot{x}_p$ and $\ddot{x}_p$ the piston position, velocity and acceleration, respectively, Q the flow entering or exiting the cylinder chamber, σ_v, F_c, F_{st} and c_{st} the parameters of the *Stribeck* model (Jelali and Kroll, 2012) (viscous coefficient, Coulomb friction force, static fiction force and characteristic velocity, respectively), and M_p, M_r and M_{oil} the masses corresponding to the piston, rod, and oil, respectively.

To maximise the energy generation of a WEC, an optimal control force (F^*_{PTO}) is generated in the controller, either via an advanced control strategy (Korde and Ringwood, 2016) or simpler resistive and reactive control strategies, as in the present case, used for illustration purposes. Resistive and reactive control are implemented using control parameters B_{PTO} and K_{PTO} as in Eq. (4e), with $K_{PTO} = 0$ in the resistive control case.

$$F^*_{PTO} = -\left(z_d K_{PTO} + \dot{z}_d B_{PTO}\right) \rightarrow \Delta p^* = F^*_{PTO} \,/\, A_p \tag{4e}$$

This F^*_{PTO} is then used to estimate the optimal pressure difference between the hydraulic cylinder chambers (Δp^*), which, in turn, is employed to define the fractional displacement of the hydraulic motor (α), the actual control input of the HyPTO. The fractional displacement α can vary between [-1,1], meaning that both ports in the hydraulic motor can be inlet and outlet ports.

The model of the hydraulic motor includes losses due to friction and

leakage via the Schlösser loss model (Schlöesser, 1961; Schlösser, 1968). The output flow (Q_M) and torque of the motor (T_M) can be described as follows,

$$Q_M = \alpha D_\omega \omega_M - Q_{losses} \tag{5a}$$

$$Q_{losses} = \Delta p_M C_{Q1} \tag{5b}$$

$$T_M = \alpha D_\omega \Delta p_M - T_{losses} \tag{5c}$$

$$T_{losses} = C_{T1} + C_{T2}\Delta p_M + C_{T3}\omega_M + C_{T4}\omega_M^2 \tag{5d}$$

where D_ω is the displacement of the hydraulic motor, ω_M the rotational speed of the motor shaft, Δp_M the pressure difference across the hydraulic motor, and C_{Q1}, C_{T1}, C_{T2}, C_{T3} and C_{T4} the parameters of the Schlösser loss model.

The model of the SCIG is given following the equivalent two-phase (dq) representation in (Krause et al., 2013),

$$V_{sd} = R_s i_{sd} - \omega\lambda_{sq} + L_s\frac{d}{dt}i_{sd} + L_m\frac{d}{dt}(i_{sd} + i_{rd}), \tag{6a}$$

$$V_{sq} = R_s i_{sq} + \omega\lambda_{sd} + L_s\frac{d}{dt}i_{sq} + L_m\frac{d}{dt}(i_{sq} + i_{rq}), \tag{6b}$$

$$0 = R_r i_{rd} - (\omega - \omega_r)\lambda_{rq} + L_r\frac{d}{dt}i_{rd} + L_m\frac{d}{dt}(i_{sd} + i_{rd}), \tag{6c}$$

$$0 = R_r i_{rq} + (\omega - \omega_r)\lambda_{rd} + L_r\frac{d}{dt}i_{rq} + L_m\frac{d}{dt}(i_{sq} + i_{rq}), \tag{6d}$$

where

$$\lambda_{sd} = (L_s + L_m)i_{sd} + L_m i_{rd}, \tag{6e}$$

$$\lambda_{sq} = (L_s + L_m)i_{sq} + L_m i_{rq}, \tag{6f}$$

$$\lambda_{rd} = (L_r + L_m)i_{rd} + L_m i_{sd}, \tag{6g}$$

$$\lambda_{rq} = (L_r + L_m)i_{rq} + L_m i_{sq}. \tag{6h}$$

V is the voltage, i the current, R the resistance and λ the flux. Subscripts s and r are used for the stator and rotor, respectively, while d and q refer to the direct and quadrature axes, respectively. ω and ω_r are the angular speed of the reference frame and the rotor, respectively.

The electromagnetic torque (T_e), rotational speed of the generator shaft, and active (P_e) and reactive electric power (Q_e) are given, respectively, in Eq. (6i)–(6l),

$$T_e = \frac{3N_p}{4}(\lambda_{sd} i_{sq} - \lambda_{sq} i_{sd}) \tag{6i}$$

$$\dot{\omega}_r = \frac{N_p}{2J}(T_e - T_M - B_{wind}\omega_r), \tag{6j}$$

$$P_e = \frac{3}{2}(V_{sd} i_{sd} + V_{sq} i_{sq}) \tag{6k}$$

$$Q_e = \frac{3}{2}(V_{sq} i_{sd} - V_{sd} i_{sq}) \tag{6l}$$

where N_p is the number of poles in the generator, J the shaft moment of inertia and B_{wind} the friction/windage damping.

Finally, the estimation of the generated electrical energy in the time interval $[0, T_{sim}]$ can be calculated as follows,

$$E_{gen} = \int_0^{T_{sim}} P_e dt. \tag{7}$$

6. Illustrative case study

An illustrative case study is presented to evaluate the suitability of different *rHyW2W* models and demonstrate the capabilities of the CR approach presented in this study. This illustrative example should be relatively simple to minimise the computational burden (given the large number of numerical models that are needed to analyse), but include certain characteristics to enhance nonlinear effects, so that the selection of the reduced WSHI model via the *systematic* CR approach is relevant.

Therefore, a spherical heaving point absorber (HPA) WEC of 5m diameter, restricted to heave motion for the sake of simplicity, is considered, as illustrated in Fig. 1 (c). The non-uniform cross sectional area of the spherical HPA enhances the impact of nonlinear effects, such as nonlinear Froude-Krylov (FK) forces (Penalba et al., 2017a). In any case, it should be noted that the *systematic* CR approach is able to reduce the complexity of any absorber, regardless of the number of degrees of freedom and the cross-sectional area.

The different *rHyW2W* models are analysed for a polychromatic wave of 8s peak period (T_p) and 1.5m significant wave height (H_s), which is the sea-state with the highest occurrence frequency in open-ocean test sites, such as BIMEP in the Bay of Biscay or Lisbon in the Atlantic Ocean (Babarit et al., 2012). Resistive and reactive control strategies are implemented in this study following Equation (4e), in order to assess the *rHyW2W* models under different conditions, for which the optimal B_{PTO} and K_{PTO} coefficients are obtained from (Penalba and Ringwood, 2018).

The details of the WEC, the CNWT, the HyPTO system and control parameters used in this paper are given in Table 2, and are the same as presented in (Penalba et al., 2018), where further details about the CNWT setup, *e.g.* the mesh convergence study, can be found.

Table 2
Details of the WEC, the CNWT, the HyPTO system and control parameters used in this paper.

WEC	WEC diameter	5m
PTO	WEC Mass	33.3 T
	WEC natural period	3.17 s
	Hydraulic system time-step	1 ms
	Electrical system time-step	50μs
	Cylinder piston area	140 cm^2
	Cylinder length	2m
	Motor displacement	1120 cc
	Generator rated power	74.5 kW
Resistive control	B_{PTO}	170 kN/m
Reactive control	B_{PTO}	90 kN/m
	K_{PTO}	−125 kN/m

6.1. Systematic complexity reduction

The *systematic* CR approach consists of removing or linearising different dynamics and loss models from the *HiFiWEC*. The reduced options for the WSHI and HyPTO models, referred to as *rWSHI* and *rHyPTO* models, respectively, are analysed separately. Fig. 6 (b) illustrates the different *rWSHI* and *rHyPTO* possibilities, where red circles highlight the dynamics and/or loss models removed from the *cHyPTO* implemented in the *HiFiWEC*. Adequately combining the different *rWSHI* and *rHyPTO* options, a wide variety of *rHyW2W* models can be constructed.

The *HiFiWEC* could also be simplified in a single step via a *ParaM*, which would represent the whole drivetrain from ocean waves to the electricity grid using η_w as input and P_e as output. Fig. 6 (b) illustrates that option, where y_{ParaM} represents any output of the *ParamM*. Since the *HiFiWEC* includes nonlinear effects of the WSHI and HyPTO system, a nonlinear model structure, such as KGP (Giorgi et al., 2016) or ANN models (Ringwood et al., 2015; Anderlini et al., 2017), must be chosen for the parametric model.

However, designing a single precise *ParaM* to represent the whole W2W structure may be unattainable due to the complexity of the *HiFiWEC*. The identification of the parameters of a nonlinear *ParaM* that

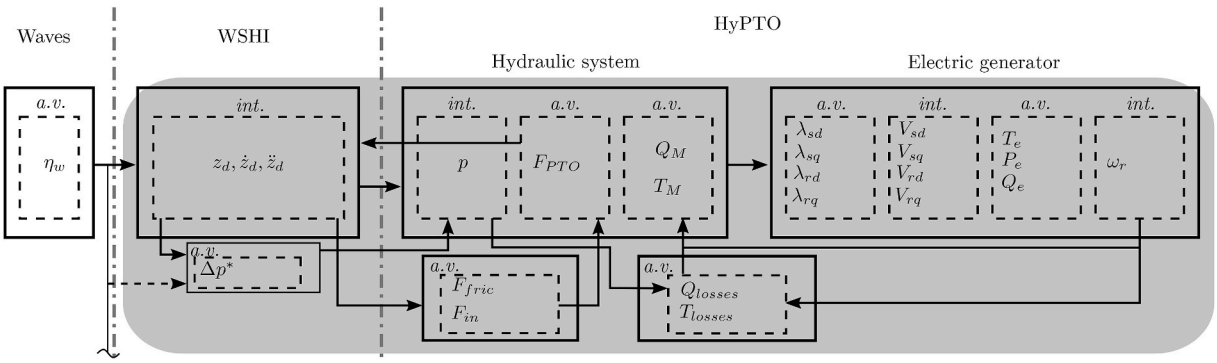

(a) The *HiFiWEC*.

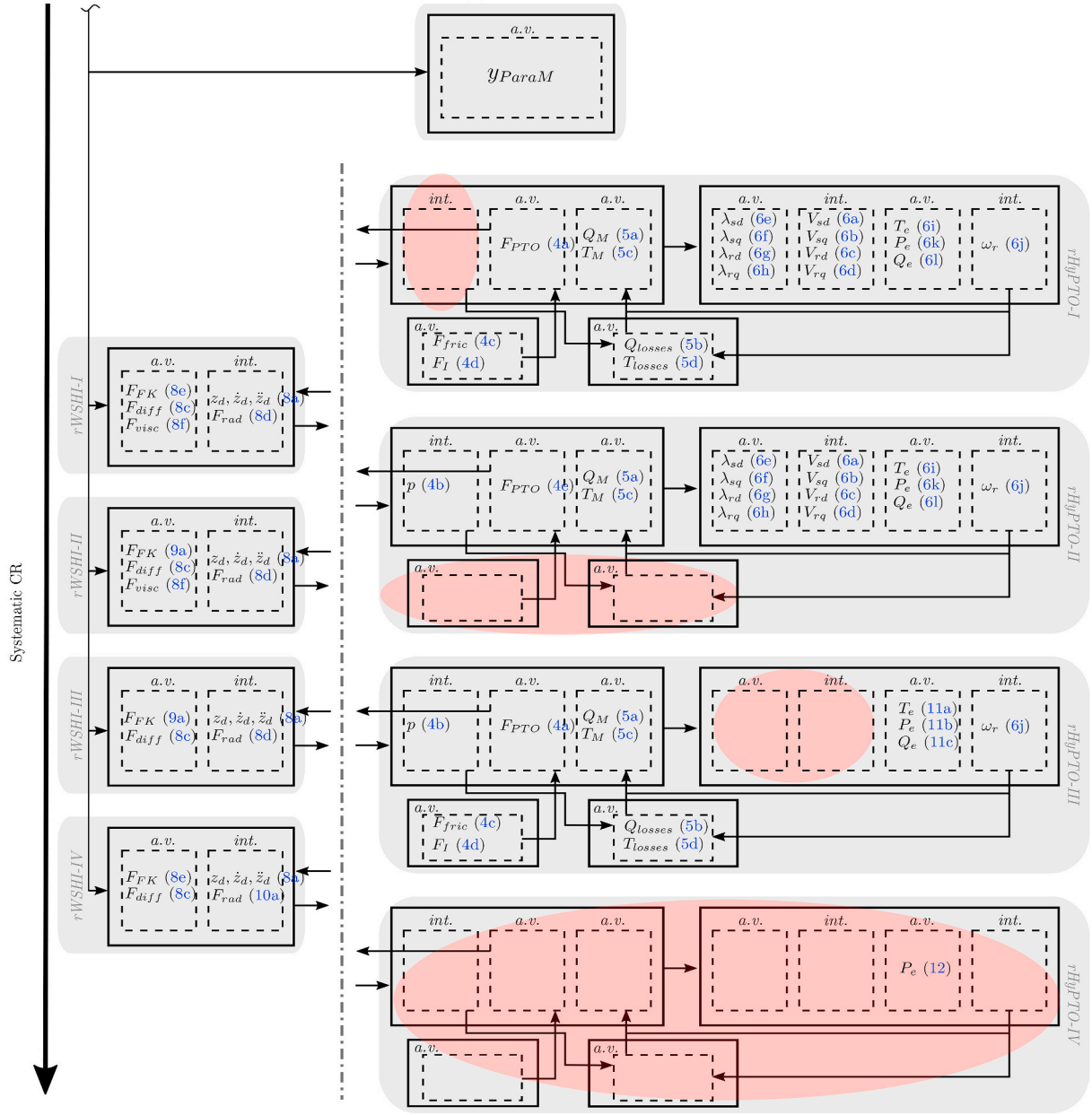

(b) Different *rWSHI* and *rHyPTO* models.

Fig. 6. Schematic illustration of the *HiFiWEC* (a) and the different CR options (b) to design *rHyW2W* models. The abbreviations *a.v.* and *int.* mean algebraic variables and integration, respectively, and red circles illustrate the part of the *cHyPTO* that has been removed. (For interpretation of the references to colour in this figure legend, the reader is referred to the Web version of this article.)

accurately covers the whole operational space of a WEC without resulting in an overly complex model, may be extremely difficult. Therefore, *ParaMs* could be used to represent only one subsystem of the drivetrain, such as the WSHI (Ringwood et al., 2016) or the efficiency of the HyPTO (Gaspar et al., 2016), or even a single effect within a subsystem, *e.g.* the fluid viscosity in the WSHI. Hence, combining a *ParaM* with other physics-based mathematical models or combining multiple *ParaMs*, each representing a single subsystem or effect, may be an option to design a mathematical model that represents the whole W2W structure.

6.1.1. WSHI reduction

Taking Equations (3a) and (3b) as the starting point and excluding *ParaMs*, a potential flow (PF) model is the next step in the progressive CR of the WSHI problem, as illustrated in Fig. 3 (a). In PF theory, the fluid is assumed inviscid and the flow irrotational and incompressible.

6.1.1.1. rWSHI-I.

Furthermore, if the divisibility of the total fluid force is assumed, Equations (3a) and (3b) can be given as follows,

$$M\ddot{z}_d = F_{fluid} + F_{PTO} + Fothers, \tag{8a}$$

where F_{others} represents other external forces, such as F_{moo}, and

$$F_{Fluid} = F_g + F_{FK} + F_{rad} + F_{diff} + F_{visc}. \tag{8b}$$

F_{FK}, F_{rad}, F_{diff} and F_{visc} represent the FK, radiation, diffraction and viscous forces, respectively. It should be noted that F_{FK} includes static and dynamic FK forces, where the static part corresponds to the buoyancy force. Since linear approximations of radiation and diffraction forces are assumed to be reasonably accurate for the spherical HPA, F_{rad} and F_{diff} can be given (Cummins, 1962) as follows

$$F_{diff} = \int_{-\infty}^{\infty} K_{diff}(t-\tau)\eta_w(\tau)d\tau, \tag{8c}$$

$$F_{rad} = -\mu_\infty \ddot{z}_d(t) - \int_{-\infty}^{t} K_{rad}(t-\tau)\dot{z}_d(\tau)d\tau \tag{8d}$$

where $K_{diff}(t)$ and $K_{rad}(t)$ are the diffraction and radiation impulse response functions (IRFs), μ_∞ is the added mass value at infinite frequency.

If the linear approximation of F_{rad} and F_{diff} does not provide a sufficiently accurate representation of the radiation and diffractions effects, a more accurate approximation of radiation and/or diffraction effects can be obtained from, for instance, the *mLPF* approach described in (Crooks, 2016).

Nonlinear FK forces and viscous effects are deemed to be necessary for the spherical HPA (Penalba et al., 2017b) and, thus, F_{FK} and F_{visc} are calculated via an algebraic solution presented in (Giorgi and Ringwood, 2017a) and a Morison-like equation (Morison et al., 1950), respectively,

$$F_{FK} = F_g - 2\pi\rho g\left[\frac{\sigma^3}{3} + z_d\frac{\sigma^2}{2}\right]_{\sigma_1}^{\sigma_2} - \frac{2\pi}{k_w}\rho g a\cos(\omega_w t)\left[\left(z_d + \frac{1}{k_w} - v\right)e^{k_w\sigma}\right]_{\sigma_1}^{\sigma_2}, \tag{8e}$$

$$F_{visc} = -\frac{1}{2}\rho\, C_d A_d(t)|\dot{z}_d - \dot{\eta_w}|(\dot{z}_d - \dot{\eta_w}), \tag{8f}$$

where g is the acceleration due to gravity, σ the parametric cylindrical coordinate of the algebraic solution to solve instantaneous F_{FK}, ω_w the wave frequency, a the wave amplitude, k_w the wavenumber, C_d the drag coefficient, and A_d the cross-sectional area of the spheric HPA at the water surface.

Hydrodynamic coefficients, such as μ_∞, K_{diff} and K_{rad}, are obtained using a boundary element method (BEM) solver, such as WAMIT (WAMIT Inc, 2013) or NEMOH (Babarit and Delhommeau, 2015), and C_d is identified from CNWT simulations. All the hydrodynamic coefficients corresponding to the spherical absorber considered in the illustrative case study described in Section 6 can be found in (Giorgi and Ringwood, 2017b).

Hence, *rWSHI-I* can be constructed using Equations (8a)-(8f), resulting in a *pNLPF* model. In addition, the convolution integral in Equation (8d) can be replaced by a computationally more efficient state-space model.

6.1.1.2. rWSHI-II.

The complexity of the WSHI problem can be further reduced, although these reductions may lead to further reductions in fidelity. F_{FK} can be linearised, replacing Equation (8e) as follows,

$$F_{FK} = \int_{-\infty}^{\infty} K_{FK}(t-\tau)\eta_w(\tau)d\tau, \tag{9}$$

where $K_{FK}(t)$ is the FK IRF. The other components in *rWSHI-II* remain the same as in *rWSHI-I*, as illustrated in Fig. 6 (b). Hence, the *rWSHI-II* model is a *viscLPF* model typically used in the literature.

6.1.1.3. rWSHI-III.

Another step in the *systematic* CR is removing viscous effects, so that *rWSHI-III* model becomes a *LPF* model.

sub*rWSHI-IV*.

Finally, the radiation force can be replaced with a *M-D* system, as in (Li and Belmont, 2014; Brekken, 2011), completely neglecting the memory effects in the WSHI,

$$F_{rad} = B_{rad}\dot{z}_d + A_{rad}\ddot{z}_d \tag{10a}$$

where B_{rad} and A_{rad} are the radiation damping and added-mass coefficient corresponding to the wave period (peak period in the case of irregular waves), respectively, obtained via a BEM solver.

6.1.2. HyPTO reduction

The *cHyPTO* model included in the *HiFiWEC* can be simplified by neglecting or simplifying specific dynamics and losses of the hydraulic system and electric generator, as shown in Fig. 6 (b). The *cHyPTO* includes a multirate solver with different time-steps (δt) used for each subsystem of the drivetrain, namely $\delta t_{WSHI} = 10ms$ for the WSHI, $\delta t_{Hyd} = 1ms$ for the hydraulic system and $\delta t_{Elec} = 50\mu s$ for the electric generator. However, the simplification or omission of certain (higher-frequency) dynamics allows the use of a larger δt, which can significantly reduce the computational cost of the *rHyW2W* model.

All the required parameters of the mathematical models for the hydraulic system (including the coefficients of the loss and friction models) and electric generator (the electrical resistances and inductances, and the inertia of the electric generator) are given in (Penalba et al., 2017c) and (Penalba et al., 2017d), respectively.

6.1.2.1. rHyPTO-I.

In *rHyPTO-I*, fluid compressibility is neglected in the hydraulic system, meaning that Δp in Equation (4b) is the same as Δp^*, which is derived from F^*_{PTO} in Equation (4e). The omission of compressibility effects allows the use of a larger δt in the hydraulic system model: $\delta t_{Hyd} = 10ms$.

6.1.2.2. rHyPTO-II.

Losses in the HyPTO system are neglected in *rHyPTO-II*. Hence, leakages, friction losses and inertia effects in the hydraulic cylinder ($F_{fric} = F_I = 0$) and motor ($Q_{losses} = T_{losses} = 0$) are neglected, meaning that $F_{PTO} = F^*_{PTO}$.

6.1.2.3. rHyPTO-III.

The complexity of the electric generator is reduced in *rHyPTO-III*, where the electric dynamics are completely neglected. Hence, *rHyPTO-III* only includes the steady-state response of the electric generator, which permits the use of a larger time-step ($\delta t_{Elec} = 10ms$), significantly reducing the computational cost.

Therefore, Equation (6a)–(6l) are replaced with their steady-state

Table 3
Configuration of the different balanced *rHyW2W* models designed in this paper.

Balanced ***rHyW2W***	WSHI		HyPTO			
	Nonlinear FK forces	Viscosity effects	Hydraulic losses	Hydraulic dynamics	Electrical losses	Electrical dynamics
rHyW2W-I	✓	✓	✓	✓	✓	✓
rHyW2W-IIa			✓	✓	✓	✓
rHyW2W-IIb		✓	✓	✓	✓	✓
rHyW2W-III	✓	✓	✓		✓	✓
rHyW2W-IV	✓	✓			✓	✓
rHyW2W-V	✓	✓	✓	✓	✓	
rHyW2W-VI	✓	✓	✓		✓	

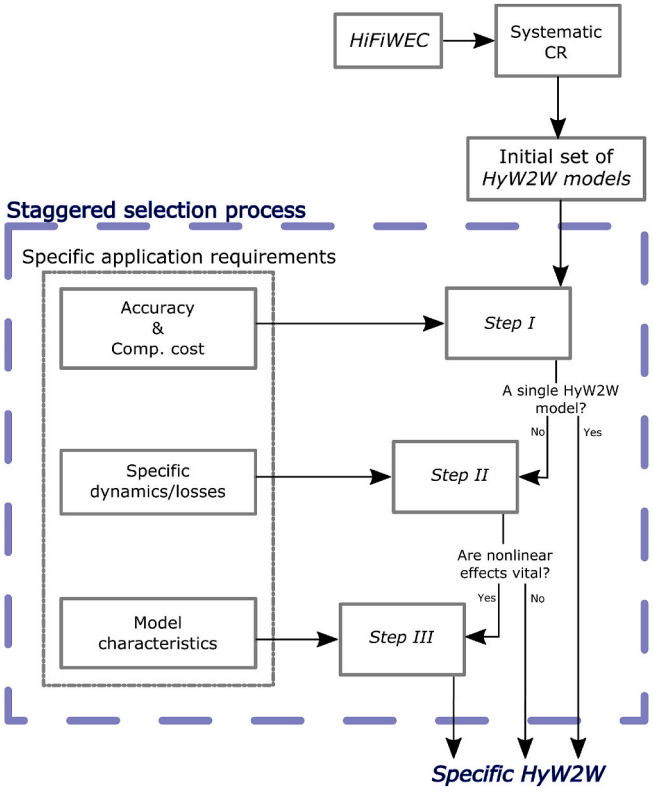

Fig. 7. Specific HyW2W model selection strategy.

representations (Hughes and Drury, 2013) as follows,

$$T_e^{ss} = \frac{3\frac{Np}{2}R_r V_g^2}{s\omega_g\left[\left(R_s + R_r + \frac{1-s}{s}R_r\right)^2 + \omega_g(L_s + L_r)^2\right]} \tag{11a}$$

$$P_e^{ss} = 3V_g I_e^{ss} cos(\angle Z^{ss}) \tag{11b}$$

$$Q_e^{ss} = 3V_g I_e^{ss} sin(\angle Z^{ss}) \tag{11c}$$

where V_g is the grid voltage, s the generator slip and ω_g the frequency of the grid voltage. The current at the stator is given as,

$$I_e^{ss} = \frac{V_g}{Z^{ss}}, \tag{11d}$$

with

$$Z^{ss} = \frac{Z_r Z_m}{Z_r + Z_m} + Z_s. \tag{11e}$$

Z_r, Z_s and Z_m are the rotor, stator and magnetizing impedances, respectively.

6.1.2.4. rHyPTO-IV. *rHyPTO-IV* is the most simplistic case, where the HyPTO is completely idealised, meaning that generated power is the same as absorbed power,

$$P_{gen} = P_{abs} = -\dot{z}_d F_{PTO}^* \tag{12}$$

6.2. Design of balanced rHyW2W models

Reduced versions of the *HiFiWEC*, designed by combining the different options suggested in Sections 6.1.1 and 6.1.2, can lead to highly unbalanced (from a complexity perspective) and/or excessively simplified HyW2W models, *e.g.* the CNWT combined with *rHyPTO-IV* (referred to as *CNWT-iPTO*) or *rWSHI-III* combined with *rHyPTO-IV* (referred to as *LBEM-iPTO*), which result in inaccurate HyW2W models (Penalba et al., 2018). In the present paper, a number of reasonably balanced *rHyW2W* models, presented in Table 3, are designed via the *systematic* CR approach.

6.3. HyW2W model selection

Among the initial set of *HyW2W* models, including the *HiFiWEC* and the balanced *rHyW2W* models shown in Table 3, the *specific HyW2W* model must be selected. Specific application requirements, presented in Table 1, are divided into three main groups: Accuracy and computational costs, specific dynamics, and losses and model characteristics. Hence, the selection process is also designed as an elimination process divided into three steps, following these three groups of specific requirements. Fig. 7 illustrates the staggered selection process to select the *specific HyW2W* model.

6.3.1. Step I

In *Step I* of the staggered selection process, the accuracy of E_{gen} estimation and the computational cost of the different HyW2W models is evaluated. The accuracy and computational cost requirements for each application are defined in Fig. 2, where the accuracy is given by the fidelity of each mathematical model compared to the *HiFiWEC*. Hence, the HyW2W models that cannot provide the required fidelity within the required computational cost are eliminated. If only one HyW2W model can meet the accuracy and computational cost requirements, then that HyW2W will be by default the *specific HyW2W* model. Otherwise, the successful *HyW2W* models are sorted from the computationally cheapest to the most expensive, before passing to *Step II*.

6.3.2. Step II

Among the *HyW2W* models that succeed to *Step II*, the inclusion of specific dynamics and losses is analysed. Hence, the *HyW2W* models that neglect the dynamics and/or losses that are specifically required by the application are eliminated in *Step II*. In case the inclusion of nonlinear effects is not a vital requirement of the application under analysis, the *HyW2W* model on the top of the list, that is, the computationally cheapest, will be chosen as the *specific HyW2W* model.

6.3.3. Step III

Finally, the degree of nonlinearity of the HyW2W models that

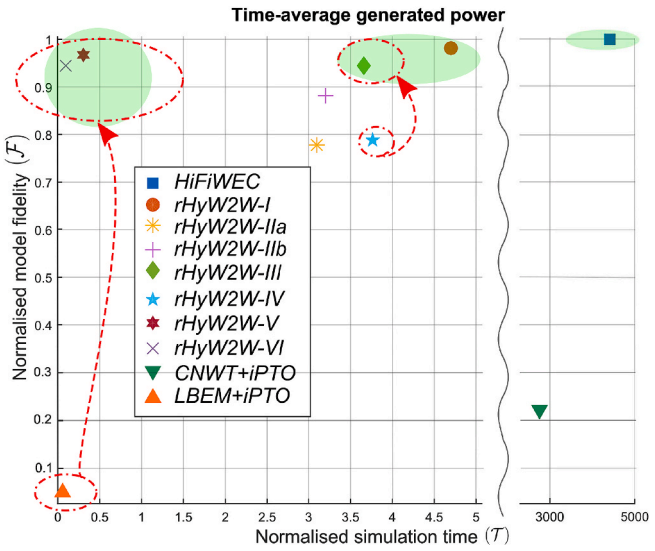

Fig. 8. Fidelity/computational cost compromise of the different HyW2W models studied in this paper.

progress to *Step III* is evaluated. These successful HyW2W models are sorted from the most nonlinear to the least, according to the nonlinearity measure χ presented in (Penalba and Ringwood, 2019).

The implication of nonlinear effects is only relevant for *Ident* and *MBC*, as shown in Table 1, but with opposite requirements. In the case of *Ident*, retaining nonlinear effects is important, so the HyW2W model on top of the list, *i.e.* the most nonlinear model, is selected. Conversely, irrelevant nonlinear effects should be avoided when designing a model for *MBC*, so the HyW2W model on the bottom of the list, *i.e.* the least nonlinear, is the chosen for *MBC*.

7. Results

For the initial step of the selection process, the fidelity of the estimated energy generation and the computational cost of the initial set of HyW2W models, shown in Table 3, are studied, where the generated energy corresponds to the final energy generated in the electric generator and delivered into the national grid.

Fig. 8 illustrates the fidelity/computational cost compromise of the HyW2W models included in the initial set, presented in Table 3, under reactive control. In addition, the unbalanced *CNWT + iPTO* and the excessively simplified *LBEM + iPTO* models are also included, for the sake of completeness. The fidelity measure ($\mathcal{F}$) is given as a normalised value, using the *HiFiWEC* as benchmark, while the computational cost is given as the ratio between the simulation time and the real time required to run the simulation $\left(\mathcal{T}_{ratio} = \frac{t_{sim}}{t_{real}}\right)$.

The extreme computational cost of the CNWT-based approaches, *i.e.* the *HiFiWEC* and the *CNWT-iPTO* model, is clearly shown in Fig. 8, which are over $\mathcal{O}$ (1000) slower than the rest of the HyW2W models. Furthermore, the substantial computational time and high-fidelity WSHI results of CNWT-based approaches do not ensure high-fidelity results of W2W models, unless the PTO system is appropriately represented, as shown in the case of the *CNWT-iPTO* model. In addition, the impact of including different aspects of the WSHI and PTO system are illustrated in Fig. 8. For instance, it is shown that including nonlinear effects into the WSHI model can substantially increase the fidelity, but that fidelity increase involves an increase in computational cost. (see the evolution from *rHyW2W-I* to *rHyW2W-IIb* to *rHyW2W-IIa*, where nonlinear effects included in the WSHI model are reduced progressively from a model that incorporates nonlinear FK forces and viscous effects, to linearise FK forces in *rHyW2W-IIb* and also removing viscous effects in *rHyW2W-IIa*).

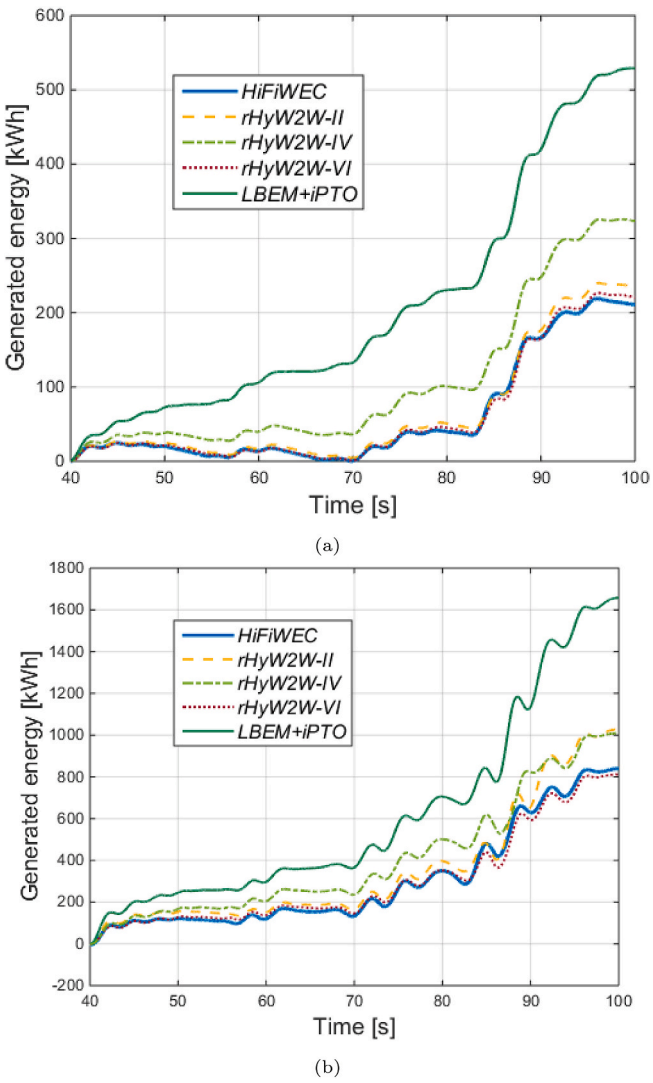

Fig. 9. Generated energy estimations of different HyW2W models under resistive (a) and reactive (b) control.

Similarly, including dynamics of the different HyPTO components has a substantial impact on the computational cost of the numerical model, but, in this case, these dynamics are irrelevant for the fidelity of the final estimation of energy generation (see differences between *rHyW2W-I*, *rHyW2W-III* and *rHyW2W-VI*, where the PTO model is reduced removing fluid compressibility dynamics in *rHyW2W-III* and also electric dynamics in *rHyW2W-VI*).

The computational cost of a given *rHyW2W* model does not vary with the implemented control strategy, that is, regardless if resistive or

Table 4
Fidelity, computational cost and nonlinearity characteristics of *rHyW2W* models, where fidelity figures in green and blue denote over- and under-estimated values, respectively (see the electronic version for the colour code).

HyW2W	$\mathcal{T}_{ratio}$	Resistive control		Reactive control	
		$\mathcal{F}$	χ	$\mathcal{F}$	χ
rHyW2W-I	4.7	0.95	0.23	0.97	0.12
rHyW2W-IIa	3.1	0.89	0.22	0.77	0.11
rHyW2W-IIb	3.2	0.93	0.22	0.89	0.12
rHyW2W-III	3.7	0.94	0.15	0.94	0.09
rHyW2W-IV	3.8	0.51	0.21	0.79	0.11
rHyW2W-V	0.31	0.95	0.23	0.95	0.12
rHyW2W-VI	0.1	0.95	0.15	0.94	0.08

reactive control is implemented, the computational cost of that *rHyW2W* model is identical. In contrast, the fidelity level of the HyW2W models may vary significantly, for example, under resistive or reactive control. Therefore, Fig. 9 (a) and (b), respectively, illustrate the E_{gen} under resistive and reactive control for the *HiFiWEC*, reduced models *rHyW2W-II*, *rHyW2W-IV* and *rHyW2W-VI*, and the *LBEM* + *iPTO*. Fig. 9 illustrates that the differences between a linear and a nonlinear model to solve WSHIs are particularly relevant under more aggressive control strategies (*i.e.* reactive control), which is consistent with the conclusions found in other studies like (Penalba and Ringwood, 2019) and (Giorgi and Ringwood, 2017b), while the simplification of the HyPTO model leads to poor results under any type of control. Fidelity and computational cost of all the *rHyW2W* models, under resistive and reactive control, are presented in Table 4.

Fidelity values in Table 4 correspond to normalised absolute error values, meaning that it cannot be determined whether each *rHyW2W* model under- or overestimates energy generation. However, Fig. 9 provides that information illustrating that all *rHyW2W* models overestimate the energy generation under resistive control, while *rHyW2W-VI* is the only reduced model that provides (slightly) underestimated energy generation values under reactive control. In order to visually show this information in Table 4, overestimated values are shown in green colour, while underestimated results are given in blue colour.

Although maximum fidelity can only be achieved with the *HiFiWEC*, Fig. 8 and Table 4 show that reasonably high-fidelity results can also be obtained for a small fraction of the computational time required by the *HiFiWEC*. In fact, most of the *rHyW2W* models suggested in Table 3 provide fidelity values of over 90% under resistive and reactive control, with computational time reductions of at least three orders of magnitude compared to the *HiFiWEC*. The only exceptions that return fidelity values below 90% are the reduced models *rHyW2W-IIa* and *rHyW2W-IV*, which neglect the nonlinear effects of the WSHI and the losses in the HyPTO system, respectively. However, it should be noted that the hydrodynamic models implemented in all the reduced HyW2W models, except for the *rHyW2W-IIa* model, use the C_d parameter which must be identified via a CNWT to ensure an acceptably accurate value. In addition, the inconsistency of C_d is demonstrated in (Penalba et al., 2018), meaning that mathematical models which use Equation (8f) to represent viscous losses of the WSHI may lose fidelity, unless C_d is adequately identified for each specific case.

Based on Table 4, the list of the HyW2W models that succeed in *Step I* of the selection process can now be defined for each application. In the case of *ValVer* and *Ident* applications, since the maximum fidelity is required, the *HiFiWEC* can be directly selected as the *specific HyW2W* model. In contrast, the list of HyW2W models that succeed in *Step I* for *SimWEC* and *PowSyst* applications includes four *rHyW2W* models, sorted from the computationally most efficient to the most demanding: *rHyW2W-VI*, *rHyW2W-V*, *rHyW2W-III* and *rHyW2W-I*. This list is reduced to just two candidates, *i.e. rHyW2W-VI* and *rHyW2W-V*, for the case of the *PTOopt*, *PowAss* and *MBC* applications.

The *specific HyW2W* model can be selected for all the applications except for *MBC* after the *Step II* of the selection process, since only one *rHyW2W* model fulfils all the requirements after *Step II*. For instance, the *SimWEC* application requires all the dynamics and losses to be included, which leaves the *rHyW2W-I* model as the only possible *specific HyW2W* model. That way, the appropriate mathematical model for *SimWEC* should include nonlinear WSHI effects, such as nonlinear FK forces and viscous effects, and all losses and specific dynamics of the PTO system.

The *PowSyst* application only requires electrical system dynamics and HyPTO losses, which are only included in models *rHyW2W-I* and *rHyW2W-III*, between which the computationally more efficient *rHyW2W-III* model is selected as the *specific HyW2W* model. Hence, nonlinear WSHI effects, all relevant losses in the PTO system and electrical system dynamics are important, but dynamics of the transmission system are not crucial to provide the fidelity level required by *PowSyst* applications.

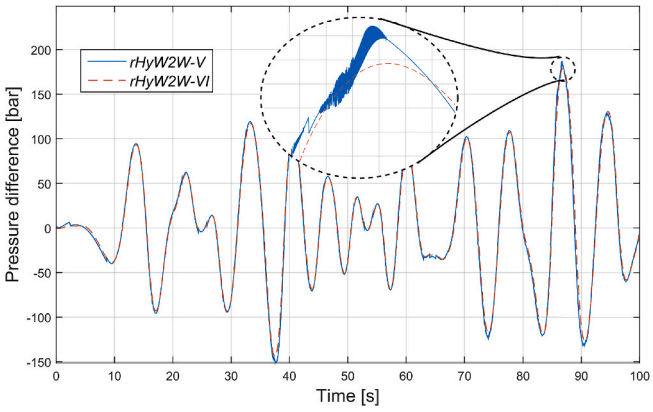

Fig. 10. Pressure difference in the hydraulic cylinder chambers modelled with *rHyW2W-V* and *rHyW2W-VI*.

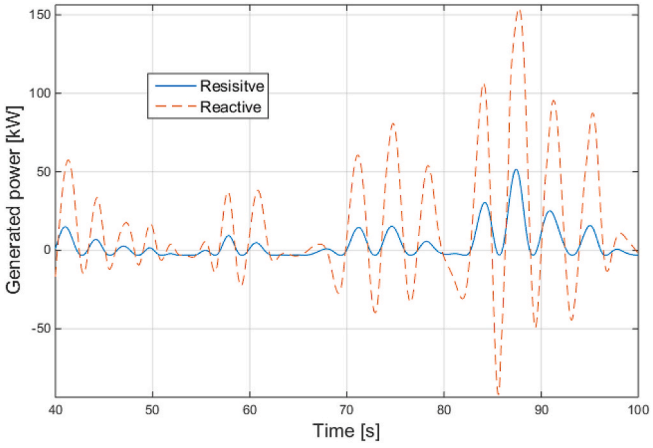

Fig. 11. Generated power profile estimated with the *rHyW2W-I* model under resistive and reactive control.

In the case of the *PTOopt* application, hydraulic system dynamics and HyPTO losses need to be considered, which are only covered by the *rHyW2W-V* model. Although the outputs from the *rHyW2W-V* and *rHyW2W-VI* models are almost identical at first glance, high-frequency dynamics, only covered by the *rHyW2W-V* model, as illustrated in Fig. 10, have a significant impact on the wear of hydraulic components. Therefore, *rHyW2W-V* is the *specific HyW2W* model for the *PTOopt* application. Therefore, mathematical models designed for *PTOopt* should ideally include nonlinear WSHI effects, losses in the whole PTO system and dynamics of the transmission system, but dynamics of the electrical system are not necessary and should be avoided to reduce the computational cost of the model.

All the requirements for the *PowAss* application are included in the two candidates that progressed to *Step II*. Therefore, the *rHyW2W-VI* model is the *specific HyW2W* model for the *PowAss* application, due to its more appealing computational cost compared to the *rHyW2W-V* model. In fact, Table 4 shows that the *rHyW2W-VI* model can provide high fidelity results (always above 95% fidelity) reducing the computational cost by one order of magnitude, compared to *rHyW2W-I*. In conclusion, nonlinear WSHI effects and losses in the whole PTO system are crucial for *PowAss*, but dynamics of the transmission and generation systems are not essential and, thus, should be avoided to obtain a computationally efficient mathematical model.

Finally, the *specific HyW2W* model for *MBC* application is selected in *Step III*, where the nonlinearity degree of the models is taken into consideration. Table 4 presents the χ measure for the different *rHyW2W* models, where all the χ measures are relatively low. In addition, the χ

Table 5
The *specific HyW2W* model for each application.

	ValVer	Ident	SimWEC	PowSyst	PTOopt	PowAss	MBC
Specific HyW2Wmodel	*HiFiWEC*	*HiFiWEC*	*rHyW2W-I*	*rHyW2W-III*	*rHyW2W-V*	*rHyW2W-VI*	*rHyW2W-VI*

measure for the same model is different when the WEC operates under resistive and reactive control and, in contrast to the overall conclusion presented in (Penalba and Ringwood, 2019), χ is higher under resistive control than under reactive control. This is linked to the power production profile of the WEC under resistive and reactive control in this particular case, shown in Fig. 11 for the *rHyW2W-I* model. The WEC under resistive control cannot produce enough energy to overcome the inertia of the electric generator at several points of the simulation, which results in a generated power profile with rather flat troughs, as shown in Fig. 11. This profile with flat troughs represents a more nonlinear behaviour of the WEC than the profile shown under reactive control, which explains the higher χ values under resistive control. Fidelity and computational cost characteristics of the *rHyW2W-V* and *rHyW2W-VI* models are very similar, but the *rHyW2W-V* model is more nonlinear, under both resistive and reactive control (up to 30% more). Therefore, the *rHyW2W-VI* model is considered as the *specific HyW2W* model for *MBC*. Hence, similarly to the *PowAss*, the mathematical model designed for *MBC* should include nonlinear WSHI effects and losses in all the different components of the PTO system, but specific dynamics of the transmission and generation systems should be avoided in order to avoid unnecessary computational cost.

Table 5 shows the *specific HyW2W* model selected for each application following the *systematic* CR approach. Hence, the objective of this paper in reducing the complexity of high-fidelity HyW2W models, while retaining the specific fidelity required by each application, illustrated by the red arrows in Fig. 2, is successfully accomplished, as illustrated by similar red arrows in Fig. 8. This complexity reduction enables to obtain mathematical models that fulfil fidelity and computational cost requirements for each application by including only the most relevant nonlinear effects, dynamics and losses.

8. Conclusions

This paper presents a *systematic* complexity reduction approach to reduce the complexity of a comprehensive high-fidelity wave-to-wire simulation platform (*HiFiWEC*), so that wave-to-wire models can be used in applications where the *HiFiWEC* is computationally too expensive, and excessively simplified computationally appealing wave-to-wire models are not accurate enough. The present paper focuses on wave-to-wire models using a heaving point absorber wave energy converter, that include a hydraulic power take-off system, but the *systematic* complexity reduction approach can easily be adapted to wave-to-wire models with other types of power take-off system.

Complexity reduction of the wave-structure hydrodynamic interaction model is one of the essential parts, due to the computationally expensive CFD-based numerical wave tanks. However, an excessive simplification, where all the different forces acting on the device are assumed to be linear, can result in excessively poor results, particularly when the wave energy converter is brought to resonance with the incident waves via an active control strategy. In order to efficiently retain the high-fidelity properties of the wave-structure hydrodynamic interaction, it is vital to identify the force components of the wave-structure hydrodynamic interaction which can be accurately approximated by a linear representation and which force components require nonlinear extensions. The nonlinear representation of the Froude-Krylov force and the inclusion of a quadratic viscous model (with an adequately identified coefficient) provide reasonably high-fidelity results for heaving point absorbers. However, nonlinear representations of other effects may be important for other types of wave energy converter.

A parsimonious representation of the power take-off system is also crucial, including only the dynamics that are vital to a particular application, and avoiding the extra computational cost due to the implementation of irrelevant dynamics. Indeed, an accurate representation of the power take-off system is demonstrated to be more important, compared to wave-structure hydrodynamic model, to obtain high-fidelity results and reduce the complexity of the wave-to-wire model. In that sense, losses of the power take-off system are the only essential part in hydraulic power take-off systems, which barely increase the complexity of the wave-to-wire model. Other specific dynamics, such as compressibility effects or electrical dynamics, should be neglected, in general, unless the application specifically requires these dynamics, since the computational cost of a wave-to-wire model can rise significantly for a similar fidelity level in the generated energy estimate.

In the cases where the implication of nonlinear effects is important, *e.g.* in the design of upper-level energy maximising control strategies, including high-frequency dynamics of hydraulic systems, such as the compressibility of the hydraulic fluid, can considerably increase the complexity of the model. Therefore it may be hard to justify this added complexity in the power take-off system model, since it significantly exceeds that of the hydrodynamic model.

Hence, it is concluded that mathematical models designed for validation/verification and identification purposes should incorporate all the possible nonlinear effects, dynamics and losses of the system, since the highest fidelity is required and computational cost is irrelevant. However, computational cost is relevant in numerical models designed for the simulation of wave energy converters, but relatively high fidelity is still needed. This requires incorporating only the most relevant effects, such as nonlinear hydrodynamic effects via the potential flow method, and losses and specific dynamics of the different components included in the power take-off system. Power system modelling and power quality analyses require mathematical models that include electrical dynamics, but the final generated energy estimation should also be as precise as possible, which necessitates considering nonlinear hydrodynamic effects and losses in the different components of the power take-off system. In contrast, mathematical models designed for power take-off component optimisation only need the dynamics of the transmission system, neglecting electrical dynamics in order to avoid unnecessary computational costs, and also require nonlinear hydrodynamic effects and losses in the power take-off system to obtain accurate energy generation estimates. Finally, requirements of the power assessment and model-based control applications are similar, *i.e.* relatively high-fidelity and very low computational cost, so the mathematical models designed for these purposes need to incorporate nonlinear hydrodynamic effects and losses in the power take-off system, but neglect the specific dynamics of the PTO components.

Acknowledgment

This material is based upon works supported by the Science Foundation Ireland under Grant No. 13/IA/1886.

References

Amundarain, M., Alberdi, M., Garrido, A.J., Garrido, I., 2011. Modeling and simulation of wave energy generation plants: output power control. IEEE Trans. Ind. Electron. 58 (1), 105–117.
Anderlini, E., Forehand, D., Bannon, E., Abusara, M., 2017. Reactive control of a wave energy converter using artificial neural networks. Int. J. Mar. Energy 19, 207–220.
Antoulas, A.C., 2005. Approximation of Large-Scale Dynamical Systems. Advances in Design and Control. SIAM, Philadelphia, PA, USA.
Antoulas, A.C., Sorensen, D.C., Gugercin, S., 2001. A survey of model reduction methods for large-scale systems. Contemp. Math. 280, 193–220.

Astolfi, A., 2010. Model reduction by moment matching for linear and nonlinear systems. IEEE Trans. Automat. Contr. 55 (10), 2321–2336.
Babarit, A., Delhommeau, G., 2015. Theoretical and numerical aspects of the open source BEM solver NEMOH. In: 11th European Wave and Tidal Energy Conference. EWTEC, Nantes, France, pp. 1–12, 08C1.
Babarit, A., Laporte-Weywada, P., Mouslim, H., Clement, A.H., 2009. On the numerical modelling of the nonlinear behaviour of a wave energy converter. In: ASME. Proceedings of the 28th Intl. Conf. On Ocean, Offshore and Artic Engineering, vol. 4. OMAE, Honolulu, pp. 1045–1053.
Babarit, A., Hals, J., Muliawan, M.J., Kurniawan, A., Moan, T., Krokstad, J., 2012. Numerical benchmarking study of a selection of wave energy converters. Renew. Energy 41, 44–63.
Bailey, H., Ortiz, J.P., Robertson, B., Buckhamn, B.J., Nicoll, R.S., 2014. A methodology for wave-to-wire WEC simulations. In: Proceedings of the 2nd Marine Energy Technology Symposium, Seattle (USA), pp. 1–15.
Bailey, H., Robertson, B.R., Buckham, B.J., 2016. Wave-to-wire simulation of a floating oscillating water column wave energy converter. Ocean Eng. 125, 248–260.
Brekken, T.K.A., 2011. On model predictive control for a point absorber wave energy converter. IEEE Trondheim PowerTech 1–8, 2011.
Cargo, C.J., Hillis, A.J., Plummer, A.R., 2014. Optimisation and control of a hydraulic power take-off unit for a wave energy converter in irregular waves. Proc. IME J. Power Energy 228 (4), 462–479.
Cargo, C.J., Hillis, A.J., Plummer, A.R., 2016. Strategies for active tuning of Wave Energy Converter hydraulic power take-off mechanisms. Renew. Energy 94, 32–47.
Cheng, D., Hu, X., Shen, T., 2010. Linearization of nonlinear systems. In: Analysis and Design of Nonlinear Control Systems. Springer, pp. 279–313.
Crooks, David, 2016. Nonlinear Hydrodynamic Modelling of an Oscillating Wave Surge Converter. Ph.D. thesis. Queens University Belfast.
Cummins, W.E., 1962. The Impulse Response Function and Ship Motions. Tech. rep., DTIC Document.
Davidson, J., Giorgi, S., Ringwood, J.V., 2015. Linear parametric hydrodynamic models for ocean wave energy converters identified from numerical wave tank experiments. Ocean Eng. 103, 31–39.
Edenhofer, O., Pichs-Madruga, R., Sokona, Y., Seyboth, K., Eickemeier, P., Matschoss, P., Hansen, G., Kadner, S., Schlömer, S., Zwickel, T., Stechow, C.V., 2011. IPCC special report on renewable energy sources and climate change mitigation. Intergovern. Panel Clim. Chang. 246.
Faedo, N., Scarciotti, G., Astolfi, A., Ringwood, J.V., 2018. Energy-maximising control of wave energy devices using a moment-domain representation. Contr. Eng. Pract. 81, 85–96.
Falcão, A.d.O., 2010. Wave energy utilization: a review of the technologies. Renew. Sustain. Energy Rev. 14 (3), 899–918.
Fiévez, J., Sawyer, T., 2015. Lessons learned from building and operating a grid connected wave energy plant. In: Proceedings of the 11th European Wave and Tidal Energy Conference, Nantes, pp. 1–6, 08D1.
Forehand, D.I., Kiprakis, A.E., Nambiar, A.J., Wallace, A.R., 2015. A fully coupled wave-to-wire model of an array of wave energy converters. IEEE Trans. Sustain. Energy 99, 1–11.
Garcia-Rosa, P.B., Vilela Soares Cunha, J.P., Lizarralde, F., Estefen, S.F., Machado, I.R., Watanabe, E.H., 2014. Wave-to-wire model and energy storage analysis of an ocean wave energy hyperbaric converter. IEEE J. Ocean. Eng. 39 (2), 386–397.
Garrido, A.J., Otaola, E., Garrido, I., Lekube, J., Maseda, F.J., Liria, P., Mader, J., 2015. Mathematical modeling of oscillating water columns wave-structure interaction in ocean energy plants. Math. Probl Eng. 2015 (727982), 11.
Gaspar, J.F., Kamarlouei, M., Sinha, A., Xu, H., Calvário, M., Faÿ, F.X., Robles, E., Soares, C.G., 2016. Speed control of oil-hydraulic power take-off system for oscillating body type wave energy converters. Renew. Energy 97, 769–783.
Giorgi, G., Ringwood, J.V., 2017a. Computationally efficient nonlinear Froude–Krylov force calculations for heaving axisymmetric wave energy point absorbers. J. Ocean Eng. Mar. Energy 3 (1), 21–33.
Giorgi, G., Ringwood, J.V., 2017b. Nonlinear froude-krylov and viscous drag representations for wave energy converters in the computation/fidelity continuum. Ocean Eng. 141, 164–175.
Giorgi, S., Davidson, J., Ringwood, J.V., 2015. Identification of nonlinear excitation force kernels using numerical wave tank experiments. In: Proceedings of the 11th European Wave and Tidal Energy Conference, European Wave and Tidal Energy Conference 2015.
Giorgi, S., Davidson, J., Ringwood, J.V., 2016. Identification of wave energy device models from numerical wave tank data - part 2: data-based model determination. IEEE Trans. Sustain. Energy 7 (3), 1020–1027.
Glover, K., 1984. All optimal hankel-norm approximations of linear multivariable systems and their L error bounds. Int. J. Contr. 39 (6), 1115–1193.
Grilli, S.T., Guyenne, P., Dias, F., 2001. A fully non-linear model for three-dimensional overturning waves over an arbitrary bottom. Int. J. Numer. Methods Fluid. 35 (7), 829–867.
Hansen, R.H., Andersen, T.O., Pedersen, H.C., 2011. Model based design of efficient power take-off systems for wave energy converters. Proc. 12th Scandinavian Int. Conf. Fluis Power 1–15.
Hansen, R.H., Andersen, T.O., Pedersen, H.C., Hansen, A.H., 2014. Control of a 420 kN discrete displacement cylinder drive for the wavestar wave energy converter. In: ASME. Fluid Power Systems Technology, ASME/BATH Symposium on Fluid Power and Motion Control. ASME. V001T01A021.
Henderson, R., 2006. Design, simulation, and testing of a novel hydraulic power take-off system for the pelamis wave energy converter. Renew. Energy 31 (2), 271–283.
Henriques, J., Gomes, R., Gato, L., Falcáo, A., Robles, E., Ceballos, S., 2016. Testing and control of a power take-off system for an oscillating-water-column wave energy converter. Renew. Energy 85 (Suppl. C), 714–724.
Henry, A., Doherty, K., Cameron, L., Whittaker, T., Doherty, R., 2010. Advances in the design of the oyster wave energy converter. In: RINA Marine and Offshore Energy Conference.
Hesam, E.S.J., 2014. An Approach to Reduce Order Modeling and Feedback Control for Wave Energy Converters. Master's thesis. Oregon State University.
Hughes, A., Drury, B., 2013. Electric Motors and Drives: Fundamentals, Types and Applications. Newnes.
Jelali, M., Kroll, A., 2012. Hydraulic Servo-Systems: Modelling, Identification and Control. Springer Science & Business Media.
Josset, C., Babarit, A., Clément, A.H., 2007. A wave-to-wire model of the searev wave energy converter. Proc. IME M J. Eng. Marit. Environ. 221 (2), 81–93.
Kelly, J.F., Wright, W.M.D., Sheng, W., OSullivan, K., 2016. Implementation and verification of a wave-to-wire model of an oscillating water column with impulse turbine. IEEE Trans. Sustain. Energy 7 (2), 546–553.
Korde, U.A., Ringwood, J.V., 2016. Hydrodynamic Control of Wave Energy Devices. Cambridge University Press.
Krause, P.C., Wasynczuk, O., Sudhoff, S.D., Pekarek, S., 2013. Analysis of Electric Machinery and Drive Systems, third ed. IEEE Press Series on Power Engineering, Wiley-Blackwell.
Letournel, L., 2015. Développement dun outil de simulation numérique basé sur lapproche" weak-scatterer" pour létude des systèmes houlomoteurs en grands mouvements. Ph.D. thesis. Ecole Centrale de Nantes.
Li, G., Belmont, M.R., 2014. Model predictive control of sea wave energy converters–part i: a convex approach for the case of a single device. Renew. Energy 69, 453–463.
Ljung, L., 1999. System Identification: Theory for the User, second ed. Prentice Hall, Englewood Cliffs, NJ, USA.
López, I., Andreu, J., Ceballos, S., de Alegría, I.M., Kortabarria, I., 2013. Review of wave energy technologies and the necessary power-equipment. Renew. Sustain. Energy Rev. 27, 413–434.
Lucas, J., Livingstone, M., Vuorinen, M., Cruz, J., 2012. Development of a wave energy converter (WEC) design tool–application to the WaveRoller WEC including validation of numerical estimates. In: Proceedings of the 4th International Conference on Ocean Energy (ICOE).
Mérigaud, A., Ringwood, J.V., 2018. Power production assessment for wave energy converters: overcoming the perils of the power matrix. Proc. IME M J. Eng. Marit. Environ. 232 (1), 50–70.
Moore, B., 1981. Principal component analysis in linear systems: controllability, observability, and model reduction. IEEE Trans. Automatic Contr. 26 (1), 17–32.
Morison, J.R., O'Brien, M.P., Johnson, J.W., Schaaf, S.A., 1950. The forces exerted by surface waves on piles. Petrol. Trans., AIME 189, 149–157.
Mork, G., Barstow, S., Kabuth, A., Pontes, M.T., 2010. Assessing the global wave energy potential, 29th International Conference on Ocean. Offshore Arctic Eng. 447–454.
O'Sullivan, A.C., Lightbody, G., 2017. Co-design of a wave energy converter using constrained predictive control. Renew. Energy 102, 142–156. Part A.
Penalba, M., Ringwood, J.V., 2016. A review of wave-to-wire models for wave energy converters. Energies 9 (7), 506.
Penalba, M., Ringwood, J., 2018. The impact of wave-to-wire models in control parameter optimisation and power assessment. In: ASME. Proceedings of the 37th International Conference on Ocean, Offshore and Arctic Engineering. OMAE, pp. 1–10. OMAE2018-77501.
Penalba, M., Ringwood, J., 2019. Linearisation-based nonlinearity measures for wave-to-wire models in wave energy. Ocean Eng. 171, 496–504.
Penalba, M., Ringwood, J.V., 2019. A high-fidelity wave-to-wire model for wave energy converters. Renew. Energy 134, 367–378. https://doi.org/10.1016/j.renene.2018.11.040. http://www.sciencedirect.com/science/article/pii/S0960148118313600.
Penalba, M., Mérigaud, A., Gilloteaux, J.-C., Ringwood, J.V., 2017a. Influence of nonlinear froude–krylov forces on the performance of two wave energy points absorbers. J. Ocean Eng. Mar. Energy 3 (3), 209–220.
Penalba, M., Giorgi, G., Ringwood, J.V., 2017b. Mathematical modelling of wave energy converters: a review of nonlinear approaches. Renew. Sustain. Energy Rev. 78, 1188–1207.
Penalba, M., Sell, N., Hillis, A., Ringwood, J., 2017c. Validating a wave-to-wire model for a wave energy converter - Part I: the hydraulic transmission system. Energies 10 (7), 977.
Penalba, M., Cortajarena, J.-A., Ringwood, J.V., 2017d. Validating a wave-to-wire model for a Wave energy converter - Part II: the electrical system. Energies 10 (7), 1002.
Penalba, M., Davidson, J., Windt, C., Ringwood, J., 2018. A high-fidelity wave-to-wire simulation platform for wave energy converters: coupled numerical wave tank and power take-off models. Appl. Energy 226C, 655–669.
Polinder, H., Damen, M.E., Gardner, F., 2004. Linear pm generator system for wave energy conversion in the aws. IEEE Trans. Energy Convers. 19 (3), 583–589.
Ricci, P., Lopez, J., Santos, M., Ruiz-Minguela, P., Villate, J.L., Salcedo, F., Falcão, A.F.O., 2011. Control strategies for a wave energy converter connected to a hydraulic power take-off. IET Renew. Power Gener. 5 (3), 234–244.
Ringwood, J., Davidson, J., Giorgi, S., 2015. Optimising numerical wave tank tests for the parametric identification of wave energy device modelling. In: ASME. Proceedings of the 34th International Conference on Ocean, Offshore and Artic Engineering. OMAE, St. John's, Newfoundland.
Ringwood, J., Davidson, J., Giorgi, S., 2016. Numerical Modelling of Wave Energy Converters : State of the Art Techniques for Single Devices an Arrays. Academic Press, Elsevier, pp. 123–147. Ch. 7: Identifying Models Using Recorded Data.

Schlöesser, W., 1961. Mathematical Model for Displacement Pumps and Motors, Hydraulic Power Transmission, pp. 252–257.
Schlösser, W., 1968. The overall efficiency of positive-displacement pumps. In: In BHRA Fluid Power Symposium, pp. 34–48.
Singler, J.R., Batten, B.A., 2009. A proper orthogonal decomposition approach to approximate balanced truncation of infinite dimensional linear systems. Int. J. Comput. Math. 86 (2), 355–371.
Sjolte, J., Sandvik, C.M., Tedeschi, E., Molinas, M., 2013. Exploring the potential for increased production from the wave energy converter lifesaver by reactive control. Energies 6 (8), 3706–3733.
Tedeschi, E., Carraro, M., Molinas, M., Mattavelli, P., 2011. Effect of control strategies and power take-off efficiency on the power capture from sea waves. IEEE Trans. Energy Conv. 26 (4), 1088–1098.
WAMIT Inc, M., 2013. WAMIT v7.0 Manual.
Weller, H.G., Tabor, G., Jasak, H., Fureby, C., 1998. A tensorial approach to computational continuum mechanics using object-oriented techniques. Comput. Phys. 12 (6), 620–631.
Willcox, K., Peraire, J., 2002. Balanced model reduction via the proper orthogonal decomposition. AIAA J. 40 (11), 2323–2330.
Windt, C., Davidson, J., Ringwood, J., 2018a. High-fidelity numerical modelling of ocean wave energy systems: a review of computational fluid dynamics-based numerical wave tanks. Renew. Sustain. Energy Rev. 93, 610–630.
Windt, C., Davidson, J., Benazzou, A., Ringwood, J., 2018b. Performance assessment of the overset grid method for numerical wave tank experiments in the openfoam environment. In: ASME. Proceedings of the 37th International Conference on Ocean, Offshore and Arctic Engineering. OMAE.
Wu, F., Zhang, X.-P., Ju, P., Sterling, M.J., 2008. Modeling and control of aws-based wave energy conversion system integrated into power grid. IEEE Trans. Power Syst. 23 (3), 1196–1204.
Yu, Z., Falnes, J., 1995. State-space modelling of a vertical cylinder in heave. Appl. Ocean Res. 17 (5), 265–275.